Supporting Information

Tracking the Interaction of Drug Molecules with Individual Mesoporous Amorphous Calcium Phosphate/ATP Nanocomposites – An X-ray Spectromicroscopic Study

Ying-Ying Jiang [a, b, c], Zhi-Qiang Wang [c], Jia-Tang Chen [c], Jun Li [c], Ying-Jie Zhu[b], Li-Jia Liu [c], Xiao-Xuan Guo [c], Yong-Feng Hu [d], Shi-Sheng He[a], Jin Wu[b], Feng Chen*[a] and Tsun-Kong Sham*[c]*

[a] Department of Orthopedic, Spinal pain Research Institute, Shanghai Tenth People's Hospital, Tongji University School of Medicine, Shanghai, 200072, P. R. China. E-mail: fchen@tongji.edu.cn

[b] Shanghai Institute of Ceramics, Chinese Academy of Sciences, Shanghai, 200050, P. R. China. E-mail: y.j.zhu@mail.sic.ac.cn

[c] Department of Chemistry, the University of Western Ontario, London, Ontario, N6A 5B7, Canada. E-mail: tsham@uwo.ca

[d] Canadian Light Source, Saskatoon, Saskatchewan, S7N 0X4, Canada

Results and Discussion

X-ray absorption near edge structure (XANES) is an element and chemical specific technique,[1] it allows for the identification of the chemical environment of an atom via the modulation of the absorption coefficient at a given absorption threshold (edge) when the atom is present in a chemical environment as compared to a free atom.[2, 3] The chemical interaction between the drug molecules (via its function group, e.g. carboxyl in drug molecules) and the surface of the carriers can be revealed by XANES analysis on the ions (Ca^{2+}) and PO_x moiety in various phosphates in the carrier. [4-9] The chemical interaction between the functional groups in the drug and specific sites in the carrier will alter the local chemical environment of the sites in the carrier, hence the XANES spectroscopy, which will provide information on the interaction as this has been demonstrated recently.[10] For example, changes of the electronic structures of the CaP nanocarriers before and after drug loading can be tracked by comparison of their XANES spectra, thus a more comprehensive understanding of how drug molecules interacting with different functional groups in drug carriers can be obtained. This information will provide foresights into the functionalization and engineering of CaP nanocarriers to enhance drug loading capacities. It should be noted that XANES can be recorded in both total electron yield (TEY) and fluorescence yield (FLY), the former was detected with specimen current, the later with a solid-state X-ray fluorescence detector, providing surface and bulk sensitivity, respectively. Scanning transmission X-ray microscopy (STXM) images were collected in transmission mode so the absolute thickness of the sample can be obtained. STXM is a spectromicroscopic technique which allows for the detailed study of the effect of drug loading and releasing in an individual nanostructure with a spatial resolution of 30 nm.[8] This technique can not only indicate the chemical interaction between drug and carrier with spatial distribution, but also provide thickness information of drug on individual carriers.

For the STXM thickness modelling procedure, XANES spectra were obtained by converting

the signal to optical density (OD) based on Beer–Lambert law:

$$OD = -\ln\left(\frac{I_t}{I_0}\right) = \mu \cdot \rho \cdot t \quad (1)$$

where I_0 and I_t are the incident and transmitted X-ray photon flux (photons), respectively. μ is the energy dependent mass absorption coefficient ($cm^2 \cdot g^{-1}$), ρ is the density ($g \cdot cm^{-3}$) of the material, and t is the sample thickness (nm). Then these spectra were converted to absolute linear absorbance scales (optical density per nm thickness sample). The elemental linear X-ray absorption, which neglects interactions such as bonding among the atoms, is calculated by aXis2000 using equation (1) and (2):

$$\mu = \frac{N_A}{MM} \sum_i x_i \cdot \sigma_{ai} \quad (2)$$

where N_A is Avogadro's number, MM is the molecular weight of a compound containing x_i atoms of type i, σ_{ai} is the atomic photo absorption cross section (cm^2 per atom) for type i atom. Then, the thickness was obtained by comparing the OD of each pixel in a STXM image and reference spectra. In this study, silicon and carbon reference spectra were obtained by fitting the original XANES spectra to match the calculated elemental linear X-ray absorption profile: ACP ($[Ca_{1.5}(PO_4)][CaHPO_4]_{0.85} \cdot 2.46\ H_2O$: density = 3.160 $g \cdot cm^{-3}$, and thickness = 1 nm) in the pre-edge and continuum. The thickness was obtained from stack fitting with the quantitatively scaled reference spectra of 1 nm thickness.

Figure 1c shows the FTIR spectra of ACPC nanocarriers before and after drug loading, the strong peak at about 1652 cm^{-1} is assigned to the C=N bond stretching vibration, which originates from ATP molecules within the ACPC nanosphere. The peak at 1652 cm^{-1} also overlaps with the vibration of -OH (1640 cm^{-1}) from the H_2O constituent in ACPC. Peaks at 1122, 928 and 558 cm^{-1} are due to the bending vibration of PO_4^{3-} relating groups. The absorption peak at 1413 cm^{-1} is attributed to the O-H bending mode of the secondary alcohol in adenosyl- with ACPC nanocarriers or in Dox molecules. Similarly, additional peaks at 1040 cm^{-1} appeared in the spectrum of ACPC/Hb indicating that Hb molecules were well loaded on ACPC nanocarriers.

In **Figure 2a**, the pre-edge peak "A" can be ascribed to 1s → 3d transition, and the shoulder peak "B" before white line is assigned to the 1s → 4s transition. Normally dipole forbidden transitions can be observed due to the hybridization of Ca with ligand states of np-character, leading to the departure from perfect crystal symmetry. The most intense peak "C" is due to dipole allowed 1s → 4p transition of Ca atom, with the peak area proportional to the unoccupied densities of state of Ca 4p character; and the shoulder peak "D" after the main resonance is mainly from multiple scattering processes.[4, 11]

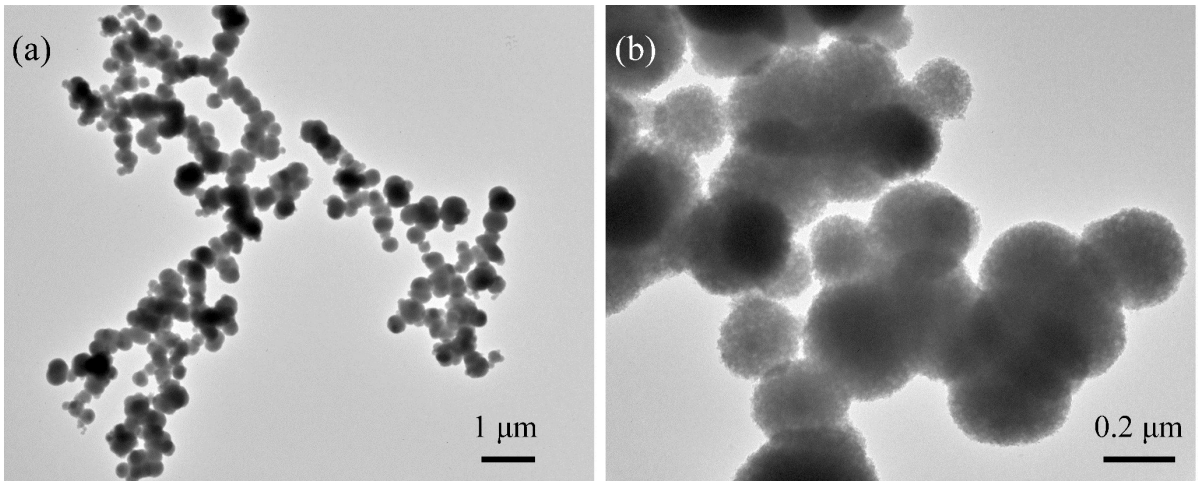

Figure S1 TEM images of ACPC nanocarriers with low magnification.

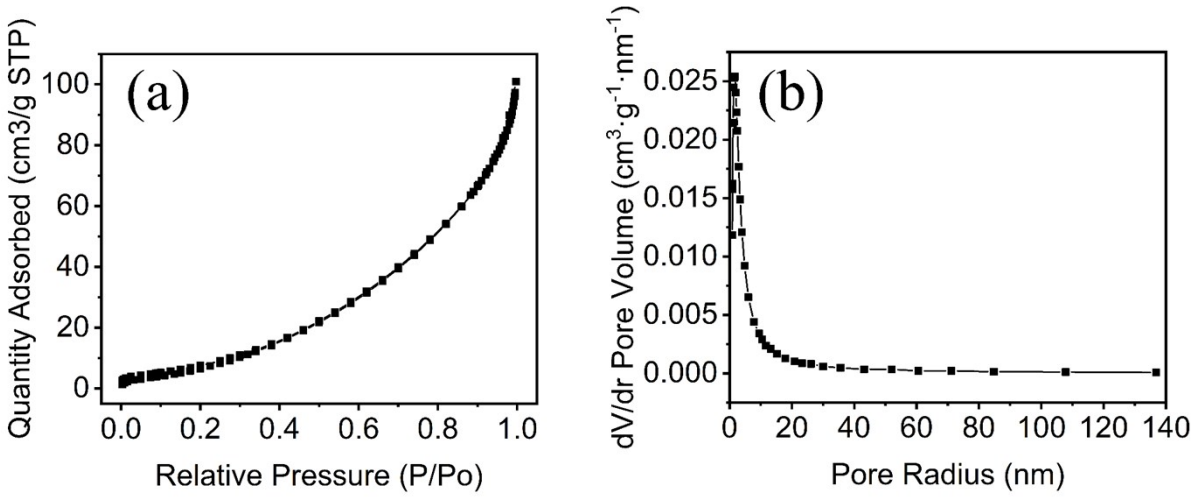

Figure S2 (a) Nitrogen adsorption-desorption isotherm and (b) BJH pore size distribution of ACPC nanocarriers

The BET specific surface area of the ACPC nanocarriers was about 42.79 $m^2 \cdot g^{-1}$, the BJH desorption cumulative pore volume and the average pore size of ACPC nanocarriers were about 0.16 $cm^3 \cdot g^{-1}$ and 3.87 nm, respectively.

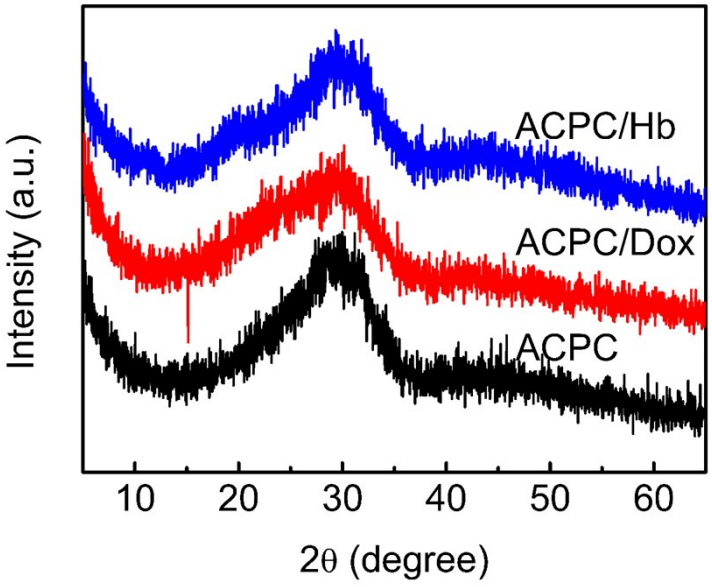

Figure S3 XRD patterns of ACPC nanocarriers before and after drug loading.

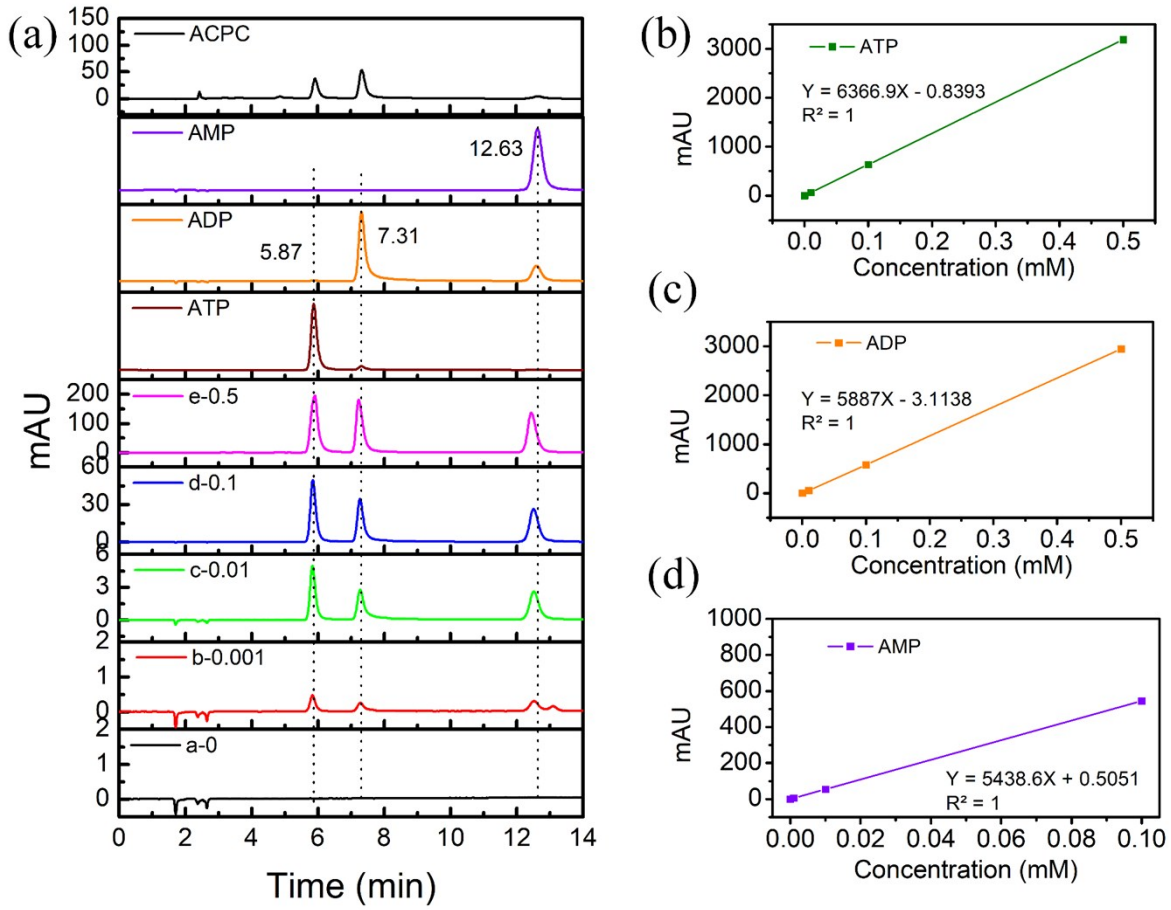

Figure S4 (a) HPLC chromatogram of ATP (remaining time 5.87 min), ADP (remaining time 7.31 min), and AMP (remaining time 12.63 min); ATP, ADP and AMP mixed solution at different concentrations, and dissolved ACPC solutions at a concentration of 0.4 mg · mL^{-1}; Related mAU-concentration curves of (b) ATP, (c) ADP and (d) AMP.

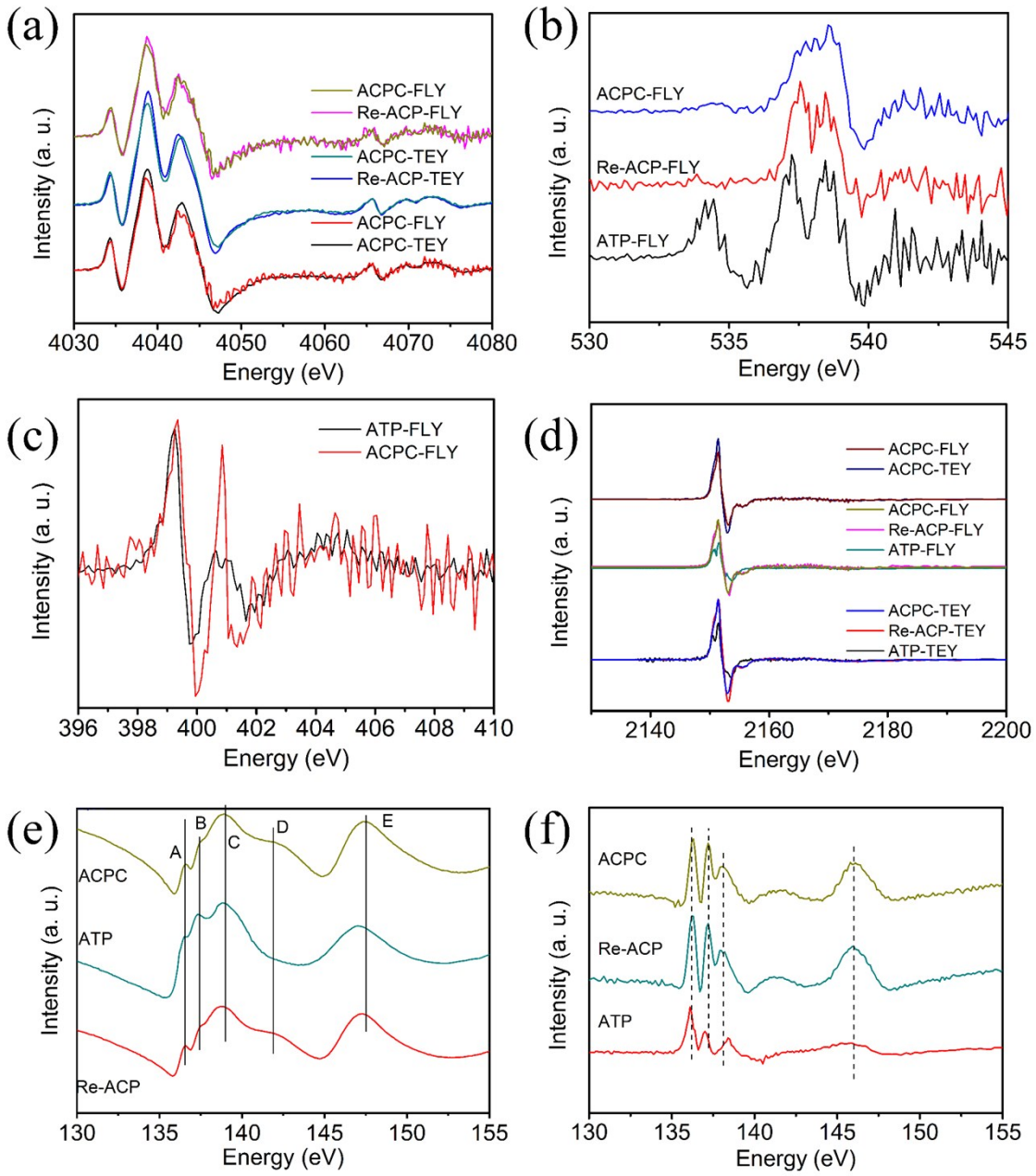

Figure S5 First derivative spectra of (a) Ca K-edge, (b) O K-edge, (c) N K-edge, (d) P K-edge and (f) P $L_{3,2}$-edge of ACPC and reference materials ACP; (e) XANES spectra of P $L_{3,2}$-edge of ACPC and reference materials ACP (Re-ACP).

The derivative spectra are the first derivative curve of the corresponding XANES spectra, they can give clearer information for energy shifts and line-shape changes in XANES spectra, so they can assist the analysis of XANES spectra.

Figure S5e shows the P $L_{3,2}$-edge XANES spectra of ACPC and the standards. The features of the P $L_{3,2}$-edge spectra are generally described by two peaks, labeled as "A" and "B" at low-energy side. These two peaks are due to transitions from spin-obit split 2p electrons (into the $2p_{3/2}$ and $2p_{1/2}$ levels) into the first unoccupied 3s-like antibonding state. Peak "C" at 138.9 eV is due to the existence of surrounding atom Ca and O. Compared with Re-ACP, peak "C" of ACPC moves to higher energy, which is close ATP.

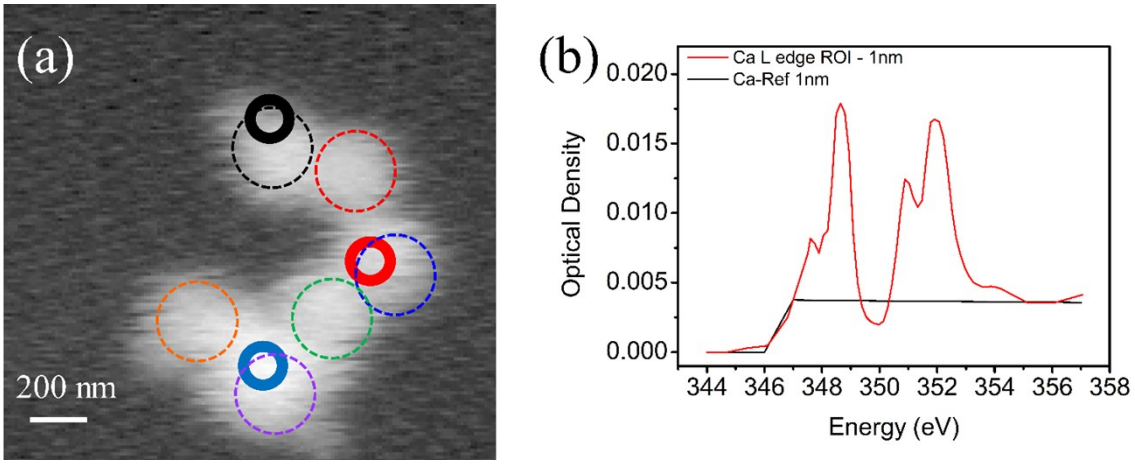

Figure S6 (a) N K-edge (dash circles show the individual nanosphere); (b) Reference spectra and elemental linear X-ray absorption profiles of ACPC (Black profile: optical density spectrum of 1 nm thickness base on formula $[Ca_{1.5}(PO_4)][CaHPO_4]_{0.85}{\cdot}2.46\ H_2O$;[12] red profile: elemental linear X-ray absorption profile).

Figure S6a shows the averaged STXM optical density images of ACPC at the O K-edge. O K-edge XANES spectra isolated from 3 different regions of interest (ROIs) on the sample were obtained and shown in **Figure S6b**. All the ROIs were selected based on the optical density (sample thickness), and there is no obvious difference in the O K-edge spectra of the three ROIs.

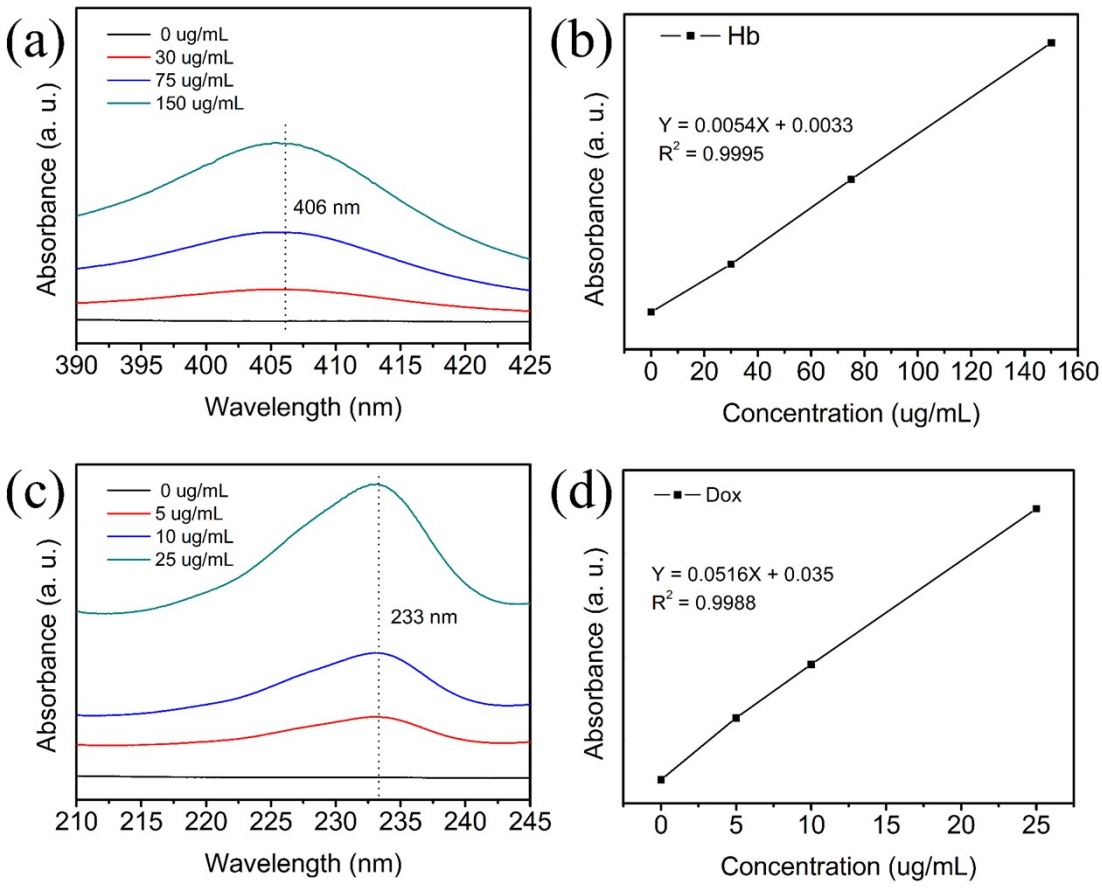

Figure S7 UV-Vis curves of (a) Hb and (c) Dox, and the corresponding Absorbance-Concentration curves (b: Hb, d: Dox).

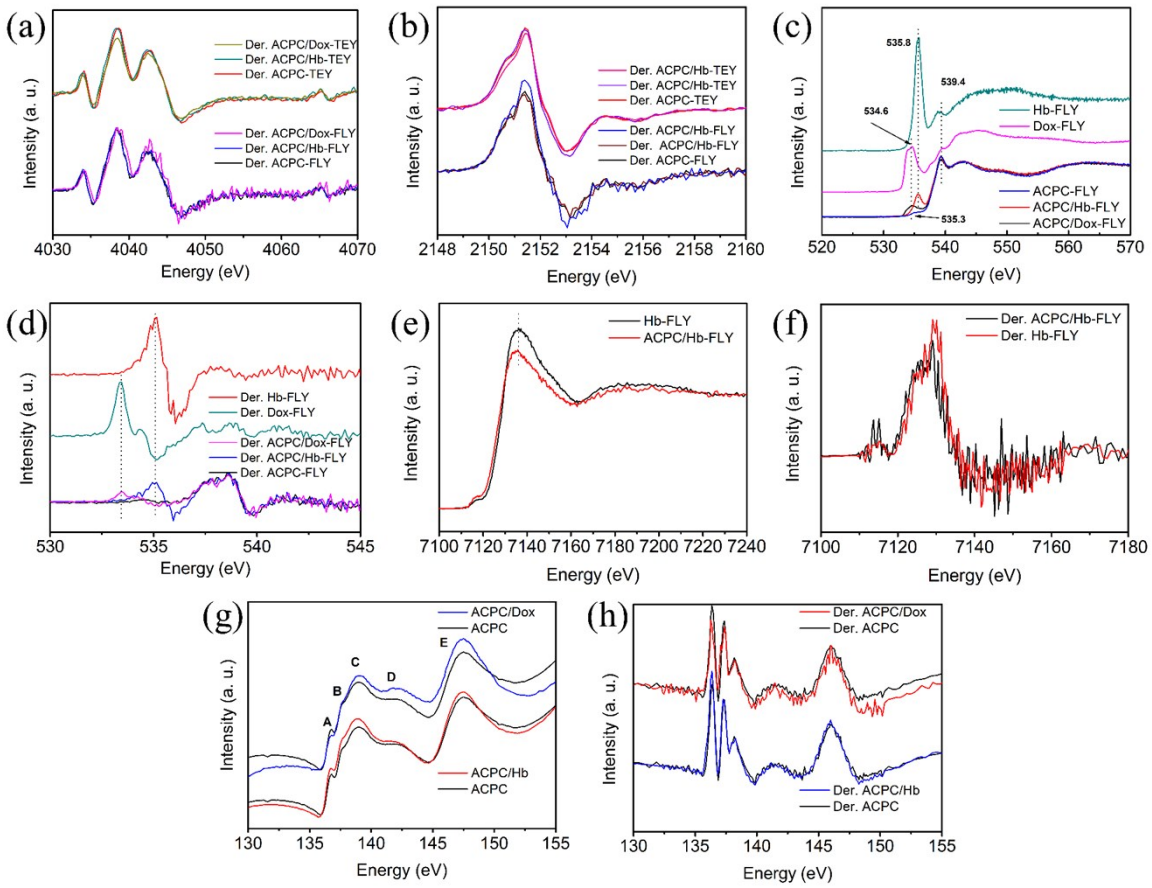

Figure S8 First derivative spectra of (a) Ca K-edge, (b) P K-edge, (d) O K-edge, (f) Fe K-edge and (h) P $L_{3,2}$-edge of ACPC before and after drug loading; XANES spectra of (c) O K-edge, (e) Fe K-edge and (g) P $L_{3,2}$-edge of ACPC before and after drug loading.

P $L_{3,2}$ -edge XANES spectra is much more sensitive for the surrounding changes of P atom. **Figure S8g** shows the P $L_{3,2}$ -edge XANES spectra in FLY mode of ACPC nanospheres before and after drug loading. Compared with ACPC, the intensity of peak "C" of the ACPC/Hb and ACPC/Dox become much stronger, which means the surrounding atom Ca or O changes after Hb/Dox loading, and this matches the conclusion got from Ca K-edge XANES spectra in **Figure 5d**.

In addition, we also collected the Fe K-edge XANES (**Figure S8e**, FLY mode) of Hb and ACPC/Hb. The white line in the spectrum of ACPC/Hb locates at 7134.6 eV, which has a red shift of 0.8 eV compared to that of Hb. It indicates that the oxidation state of Fe is a bit lower

in ACPC loaded with Hb than Hb itself. And the peak area under the curve of ACPC/Hb is reduced. In another word, there are more electrons in the surrounding of Fe atom, and the additional electrons are supposed to be donated by the interacted pyridinic N atom of adenine group within ACPC nanospheres. These changes bring it out that Hb molecules share electrons with ACPC and give a clear evidence of the interaction between Hb and ACPC nanocarriers.

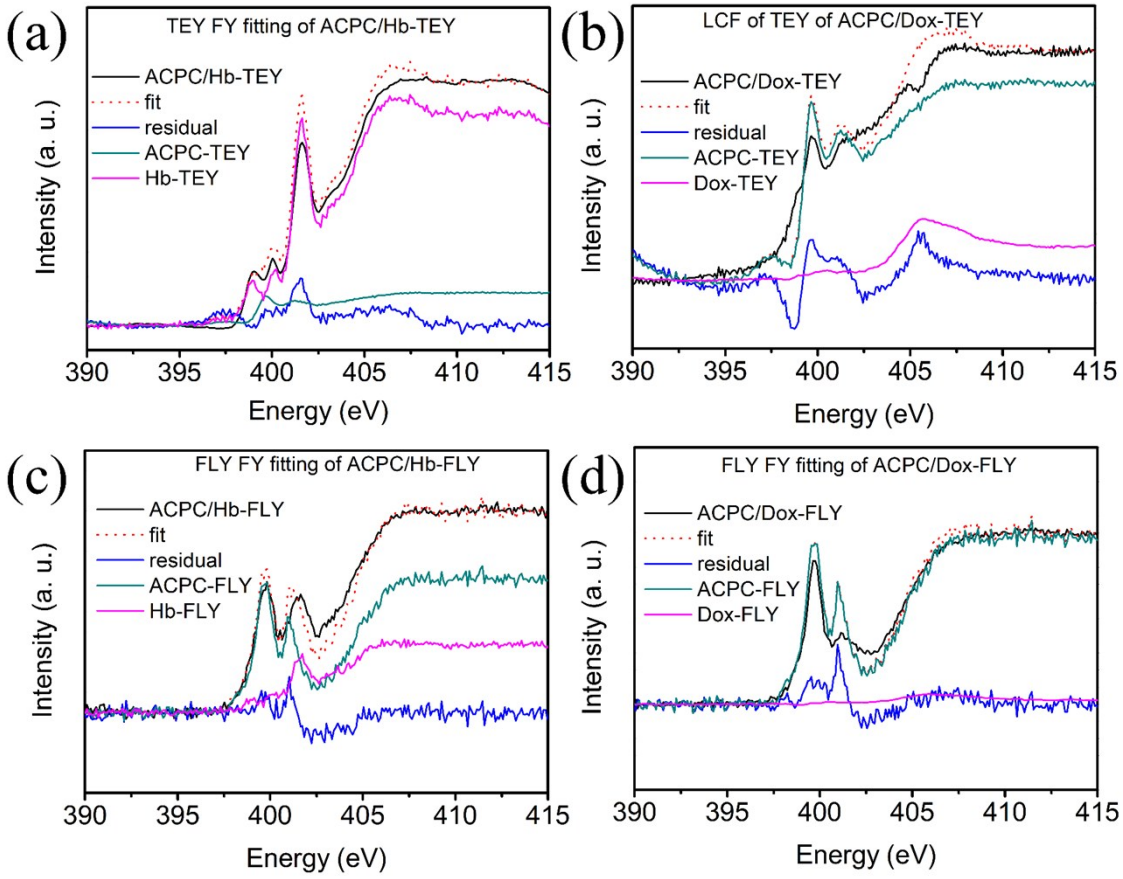

(e)

	Percentage (%)			
	ACPC	Dox	Hb	R-factor
ACPC/Hb-FLY	66.4		33.6	0.0157305
ACPC/Hb-TEY	13.4		88.6	0.0123058
ACPC/Dox-FLY	97.5	2.5		0.0190201
ACPC/Dox-TEY	86	14		0.3029140

Figure S9 N K-edge XANES spectra linear combination fitting of ACPC loaded with Hb (a: TEY; c: FLY) and Dox (b: TEY; d: FLY), and (e) related fitting results

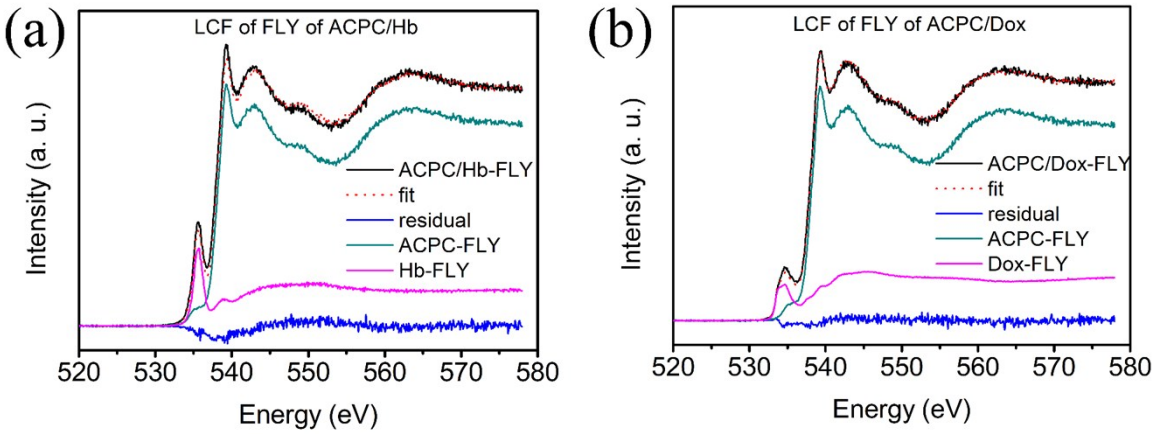

(c)

	Percentage (%)			
	ACPC	Hb	Dox	R-factor
ACPC/Hb	85.4	14.6		0.0019971
ACPC/Dox	83		17	0.0006550

Figure S10 O K-edge XANES spectra linear combination fitting of (a) ACPC/Hb, (b) ACPC/Dox, and (c) related fitting results

There are two discernible features at O K-edge XANES spectra (**Figure S8c**), the main resonance feature in the spectrum of ACPC at around 539.4 eV is due to O 1s → 2p antibonding state hybridized with orbitals of the cations which O is bound. The pre-edge peak at 535.3 eV is due to the Ca–O crystal field effects. The sharp pre-edge peaks of drug molecules are ascribed to π* resonance of O double bond, which can also be found in ACPC nanocarrier after drug loading, and the results also indicate that the drug molecules are loaded on ACPC nanocarrier. For ACPC/Dox and ACPC/Hb, there are two kind of oxide sources, one is from ACPC, the other one comes from drug molecules. LCF of XANES of ACPC/Hb and ACPC/Dox can tell the weight ratio of the carrier and drug in each sample. Herein, based on the functional groups of different drug molecules, XANES spectra of Hb, Dox and ACPC are regarded as standard

samples, and an LCF (**Figure S10a, b**) were analyzed by Athena software, and the results are listed in **Figure S10c**. From the LCF results, one can get the rough weight ratio between the ACPC carrier and drug molecules, and then calculate the loading capacity of the carrier. The LCF spectra almost overlap the original spectra of ACPC/Hb and ACPC/Dox, which indicates that no obvious chemical interaction took place at O K-edge.

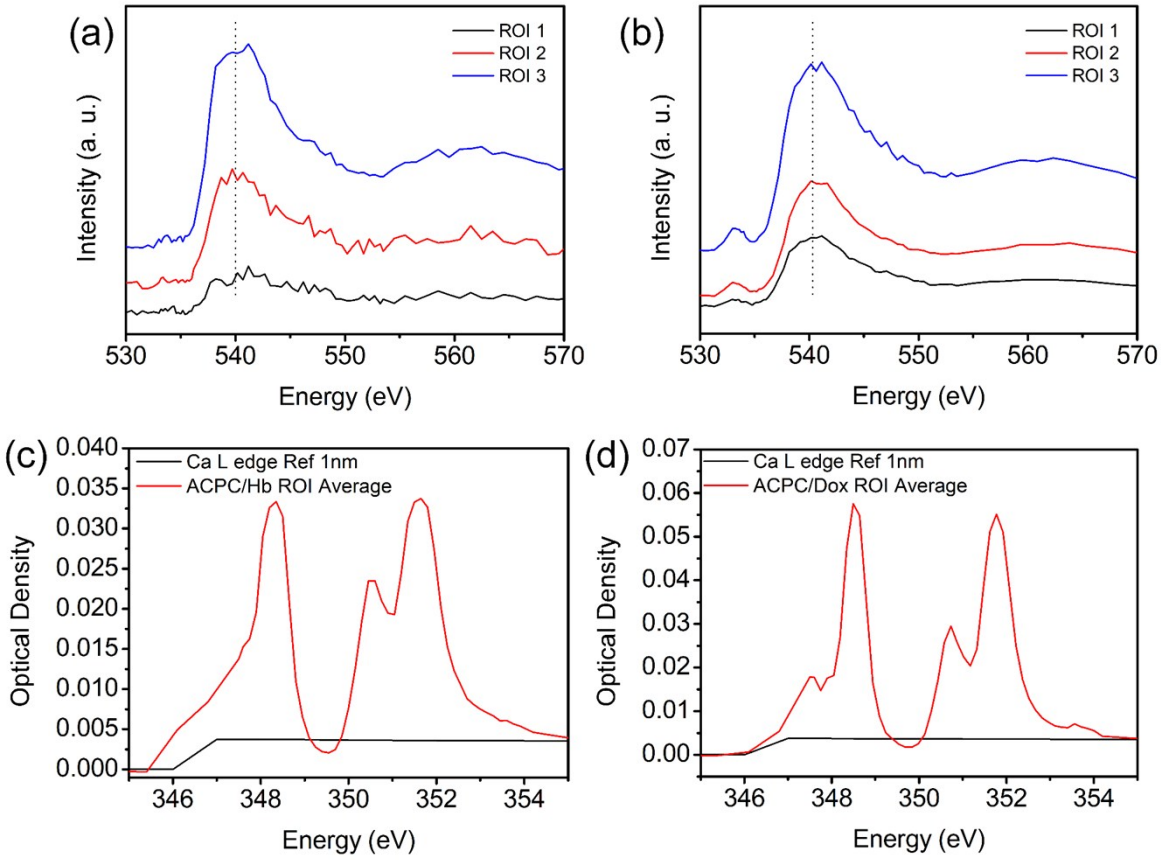

Figure S11 XANES spectra taken from each ROI (**Figure 4b, Figure 4e**) displayed in (a) ACPC/Hb and (b) ACPC/Dox at the O K-edge; Reference spectra and elemental linear X-ray absorption profiles of (c) ACPC/Hb and (d) ACPC/Dox (Black profile: optical density spectrum of 1 nm thickness base on formula $[Ca_{1.5}(PO_4)][CaHPO_4]_{0.85}\cdot 2.46\ H_2O$;[12] red profile: elemental linear X-ray absorption profile).

O K-edge XANES spectra isolated from 3 different ROIs on ACPC/Hb and ACPC/Dox were shown in **Figure S11a** and **S11b,** respectively. O K-edge XANES can reveal the presence of residual Hb or Dox and oxygen related compounds. From **Figure S11a**, the spectra of the ROIs

within ACPC/Hb nanospheres is quite similar with XANES spectra of ACPC/Hb (**Figure S10a**), but **Figure S10a** shows a more obvious pre-edge peak that comes from Hb than the spectra of ROIs shown in ACPC in **Figure S6b**. Similarly, O K-edge spectra of ROIs in **Figure S11b** also match the XANES spectrum of ACPC/Dox nanospheres shown in **Figure S10b**, meanwhile, there also appears the pre-edge peak of Dox. The result reveals the heterogeneity of ACPC/Hb and ACPC/Dox, but we cannot see obvious chemical interaction via O sites from the XANES spectra at O K-edge.

References

1. T. K. Sham, *Int. J. Nanotechnol.*, 2008, **5**, 1194-1246.
2. M. N. Banis, H. Yadegari, Q. Sun, T. Regier, T. Boyko, J. G. Zhou, Y. M. Yiu, R. Y. Li, Y. F. Hu, T. K. Sham and X. L. Sun, *Energy Environ. Sci.*, 2018, **11**, 2073-2077.
3. J. Li, J. Liu, Q. Sun, M. N. Banis, X. L. Sun and T. K. Sham, *J. Phys. Chem. C*, 2017, **121**, 11773-11782.
4. X. Guo, Z. Wang, J. Wu, Y. Hu, J. Wang, Y. J. Zhu and T. K. Sham, *Crystengcomm*, 2015, **17**, 4117-4124.
5. X. Guo, Z. Wang, J. Wu, Y. M. Yiu, Y. Hu, Y. J. Zhu and T. K. Sham, *J Phys Chem B*, 2015, **119**, 10052-10059.
6. X. Guo, J. Wu, Y. M. Yiu, Y. Hu, Y. J. Zhu and T. K. Sham, *Phys Chem Chem Phys*, 2013, **15**, 15033-15040.
7. X. M. Guo, C. Y. Wang, Y. F. Zhang, R. Y. Xia, M. Hu, C. M. Duan, Q. Zhao, L. Z. Dong, J. X. Lu and Y. Q. Song, *Tissue Eng.*, 2004, **10**, 1818-1829.
8. X. X. Guo, Z. Q. Wang, J. Wu, J. Wang, Y. J. Zhu and T. K. Sham, *Nanoscale*, 2015, **7**, 6767-6773.
9. X. X. Guo, J. Wu, Y. M. Yiu, Y. F. Hu, Y. J. Zhu and T. K. Sham, *Can. J. Chem.*, 2017, **95**, 1122-1129.
10. Y. J. Zhu, X. X. Guo and T. K. Sham, *Expert Opin. Drug Deliv.*, 2017, **14**, 215-228.
11. B. Hesse, M. Salome, H. Castillo-Michel, M. Cotte, B. Fayard, C. J. Sahle, W. De Nolf, J. Hradilova, A. Masic, B. Kanngiesser, M. Bohner, P. Varga, K. Raum and S. Schrof, *Anal. Chem.*, 2016, **88**, 3826-3835.
12. B.-Q. Lu, N. A. Garcia, D. M. Chevrier, P. Zhang, P. Raiteri, J. D. Gale and D. Gebauer, *Crystal Growth & Design*, 2019, **19**, 3030-3038.